

## Study and data analysis of turbulence numerical models in mid-atmospheric boundary layer.

Supervisors: Prof. Leonardo Primavera,  
Prof. Fabio Lepreti.

University of Calabria, Physics department, Rende (CS)

**Author:** Francesco De Rose. **ID:** 256865

2025/2026

# Introduction

- This presentation focuses on computation of the trends in the occurrence of atmospheric circulation patterns using a python script (.ipynb file).
- In the case studied, a brief explanation of the state of the art of these methods will be explained.
- All the computations and figures have been obtained using different python libraries (seaborn, xarray, scipy to name a few).

The dataset (1.9GB size) used contains 500 hPa geopotential values recorded each day at 12:00UTC from 01011980 to 11072025 relative to this area:  
 $70^{\circ}N : 35^{\circ}S$ ;  $-20^{\circ}W : 30^{\circ}E$  on an horizontal grid  $0.25^{\circ} \times 0.25^{\circ}$ .

$$\Phi = \int_0^z \mathbf{g} dz' \quad (1)$$

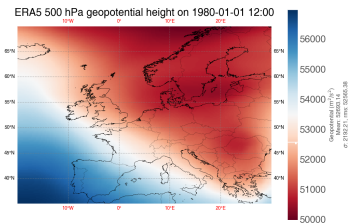
# ITFA and NWP models

The effects that climate change driven turbulence has on aviation over Europe is a serious matter, namely:

- 1 Turbulence —> microscale phenomenon . A scale mismatch makes direct forecasting extremely challenging from a meteorological standpoint.
- 2 Turbulent eddies exist across a vast spectrum of sizes . Atmospheric turbulence ranges from 100s of km down to just cm, creating complexity in prediction models.
- 3 Aircraft bumpiness peaks at aircraft scale eddies . Commercial aircraft experience the most pronounced turbulence when encountering eddies ~ 100 meters in size, roughly matching the aircraft dimensions —> No safe prediction for atmospheric motion at the 100 meter scale.
- 4 Energy cascades from larger to smaller scales . Most energy in aircraft-scale turbulent eddies originates from larger atmospheric motions that cascade downward, providing a pathway for indirect prediction.
- 5 Larger scales are observable and resolvable . Current weather observation networks and numerical weather prediction models can effectively capture and resolve these larger-scale atmospheric features.
- 6 Empirical forecasting methods bridge the scale gap . Practical "rules of thumb" can link observable large scale atmospheric patterns to aircraft-scale turbulence predictions.

## Presentation objective

The goal is to investigate the extent to which changes in atmospheric dynamics amplify the impacts of climate change on aviation turbulence at regional scales .



With long enough data (45 years) one can derive some spatial pattern of key diagnostics (mainly Ellrod's indices TI1 not TI2 [Ellrod and Knapp, 1992]) related to aviation turbulence episodes. The video shows along the colorbar the mean and RMS of the plev daily value.

This forecasting method integrates multiple turbulence diagnostics, each weighted based on observations. A set of turbulence indices are computed from

ERA5 reanalysis dataset [Faranda et al., 2024] at each grid point. Upper-level algorithms:

- I Horizontal temperature gradient;
- II Turbulence Index 1 (TI1);  
Mid-level algorithms[Sharman et al., 2006]:
  - I TI1 ;
  - II Wind speed  $\times$  horizontal deformation.
  - III many others ...

# Clear Air Turbulence (CAT) significance

## Why it's important?

CAT is defined as high-altitude aircraft bumpiness occurring away from significant cloudiness and thunderstorm activity. Nonetheless, **CAT** accounts for half of all encounters with turbulence, despite occurring in seemingly benign atmospheric conditions.

- 1 Morphology of patterns** By focusing on the morphology of large-scale **geopotential patterns**, that have become more frequent over the last four decades in ERA5 data, the most-encountered spatial patterns of key turbulence diagnostics can be identified.
- 2 Information lost** This resolution allows for the detection of temporal trends in dynamics (from hours to inter-annual decadal timescales) associated with spatial patterns, ensuring uniform spatial and temporal coverage.

See for example <https://turbli.com/maps/world-turbulence-map/>.

# Analog searching method and pseudo-code [Alberti et al., 2024]

```
procedure FINDANALOGS(maps, reference_map, q.quantile)
    distances ← empty list
    for each map.i in maps do
        distance ← EuclideanDistance(map.i, reference_map)
        distances.append(distance)
    end for
    threshold ← CalculateQuantile(distances, q.quantile)
    analogs ← empty list
    for each map.i and distance.i in maps, distances do
        if distance.i ≤ threshold then
            analogs.append(map.i)
        end if
    end for
    return analogs
end procedure

procedure ANALYZEANALOGTRENDS(analog_dates, time_interval_length)
    sub_intervals ← DivideTimeIntoSubintervals(analog_dates, time_interval_length)
    N.t ← empty list
    for each sub.interval in sub.intervals do
        count ← CountAnalogsInSubinterval(sub.interval, analog_dates)
        N.t.append(count)
    end for
    a, b ← LinearBestFit(time.points, N.t)
    return a, b
end procedure

procedure RECONSTRUCTCOMPOSITEMAPS(analog_dates, field_of_interest)
    composite_map ← empty map
    total_fields ← 0
    for each date in analog_dates do
        field_data ← RetrieveFieldData(date, field_of_interest)
        composite_map ← composite_map + field_data
        total_fields ← total_fields + 1
    end for
    composite_map ← composite_map / total_fields
    return composite_map
end procedure
```

▷ Euclidean distances  
▷ Quantile determination  
▷ Store map or its date/identifier  
▷ Trend Analysis  
▷ List to store number of analogs per sub-interval  
▷  $N(t) = at + b$   
▷ Composite map reconstruction  
▷ Sum or average fields  
▷ Average the composite map

## Figures and discussions: what's been plotted

- 1 **Annual trend** to compare the effects of climate change on plev, based on the dataset time and space indices.
- 2 **Maps at specific times**  $\Phi(\mathbf{x}, t)$  to show the overall behavior in the past 45 years.
- 3 **Contour plots** representing spatial coordinate along the horiz. plane, for a single hour of a day/month/year and the plev ( $\mathbf{x}, t$ ) as the plot intensity.
- 4 **Euclidian distances distribution and linear fits**  
For suitable reference days, the **linear fit** and **confidence interval for a consistent trend** has been computed.
- 5 **TI1** For suitable time periods, the trend for the **turbulence index** has been computed, namely the horizontal gradient of the converted geopotential.

# Tables

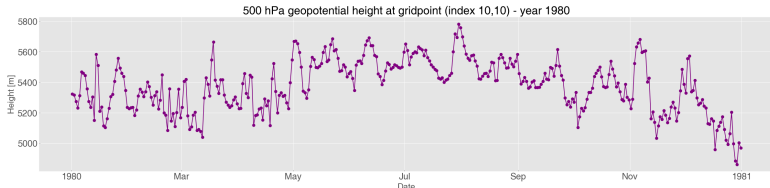
Ref.day	Analog counts	a	95% CI	q	trend
16619	1129228	17903.6	9140.8233, 26666.3767	0.98	Yes

**Table:** Coefficients and parameters for runs in the set of 5th period of 9 years 20160702-20250702. The quantiles used have been 0.98, 0.99, 0.995 as in [Alberti et al., 2024]. The dataset has been centered and standardized (each map before distance computation) to delete anomalies and seasonal variabilities in analogs computation.

Period:	80'-89'	89'-98'	98'-07'	07'-16'	16'-25'
Analog count	1059876	1083430	1124200	1123762	1129228

**Table:** Analog counts for all 5 periods 19800101-20250711. The quantiles used has been 0.98, as in [Alberti et al., 2024]; it has been chosen to highlight the 2% closest patterns . For further information refer to the "h.press.analogue.ipynb" file and the "results.fit.txt" in the directory.

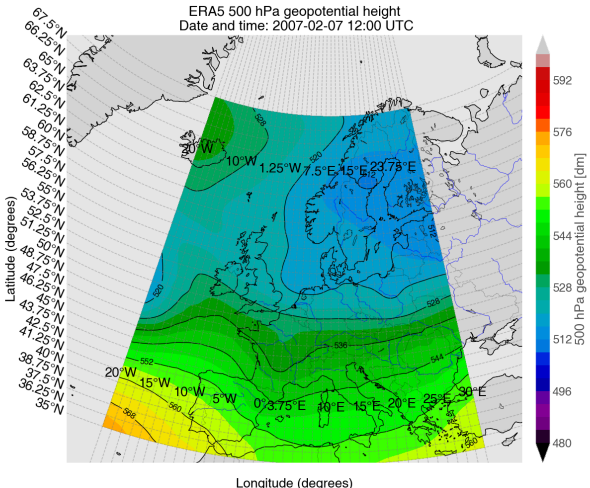
# Annual trend



Annual trend video of the 500 hPa geopotential variable plev selected at a specific index of the spatial grid. Information on the dataset:

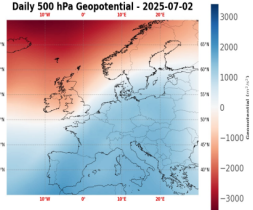
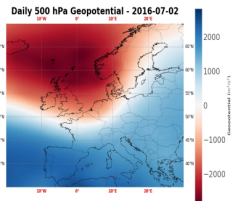
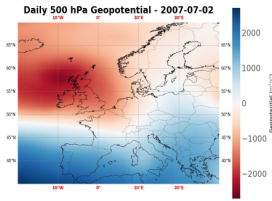
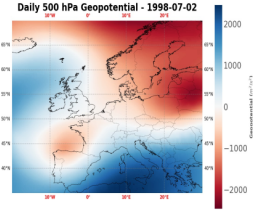
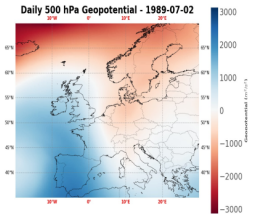
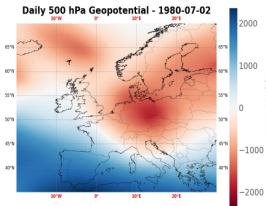
- 1 Dimensions: time: 16628 lon: 201 lat: 141 plev: 1
- 2 Coordinates: time 1980-01-01T12:00:00 ... 2025-07-11... lon -20.0 -19.75 -19.5 ... 29.75 30.0 lat 70.0 69.75 69.5 ... 35.5 35.25 35.0 plev 5e+04
- 3 Attributes: CDI : Climate Data Interface version 2.1.1  
(<https://mpimet.mpg.de/cdi>)  
Conventions : CF-1.6  
institution : European Centre for Medium-Range Weather Forecasts  
history : Tue Jul 15 20:01:00 2025: cdo -f nc4 copy data.grib data.nc  
CDO : Climate Data Operators version 2.1.1  
(<https://mpimet.mpg.de/cdo>).

# Contour plot of the 183th day of gregorian calendar

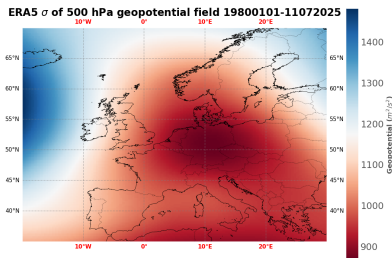
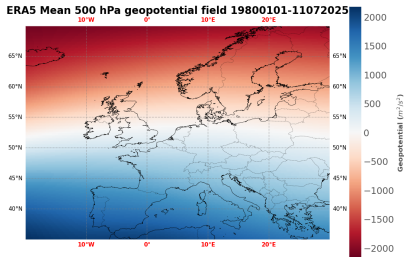


Contour plot video and closeup view of the 500 hPa geopotential variable plev selected at a specific day.

# Daily geopotential fields



# Mean and std for the whole dataset



# Analysis by means of analog method

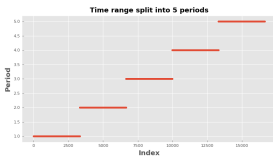
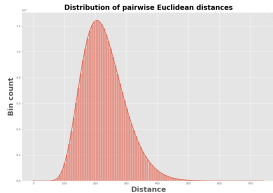
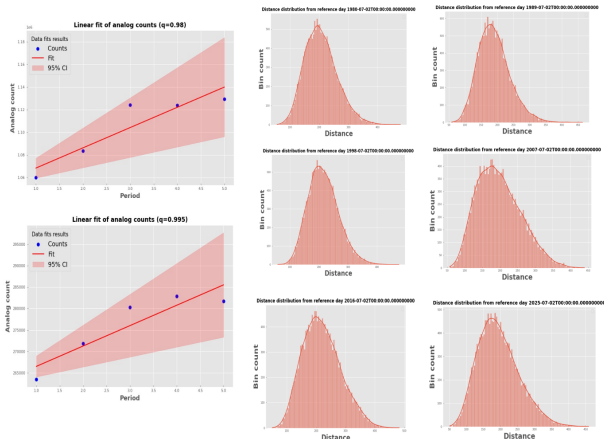


Table:  $d_{ij} = \sqrt{\sum_k (x_{ik} - x_{jk})^2}$ ,  $x_{ik}$  is the generic field value at grid point k on day i while  $d_{ij}$  measures how different two daily fields are in physical space.

# Analog metrics computation

Below Figure 5, show Euclidean distance distributions for all **six** different reference days chosen.



**Table:** Linear fit results and confidence intervals for two different quantiles reference value. Distributions of Euclidean distances for multiple map indexes at a single reference day (16691th). The linear fit has been  $N(t) = at + b$  where  $N$  is the period of years selected following the 95% CI.

# Analysis by means of analog method

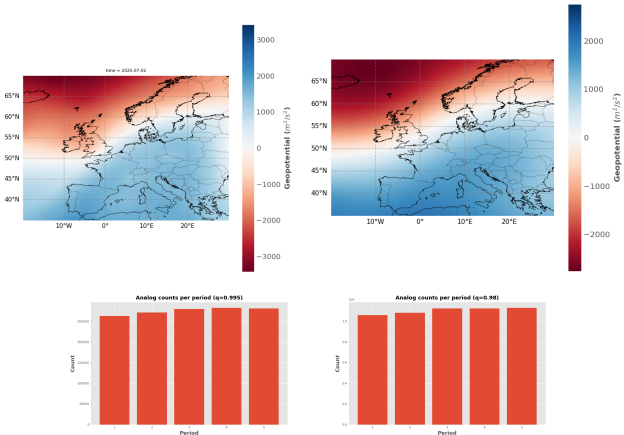


**Table:** Top images represent the analog reference map for the 16619th day and the analogs mean computed over the whole time index respectively. Bottom ones show the analogs counts for different quantiles values, the difference is not very remarkable.

# TI1 index throughout the recurrent days

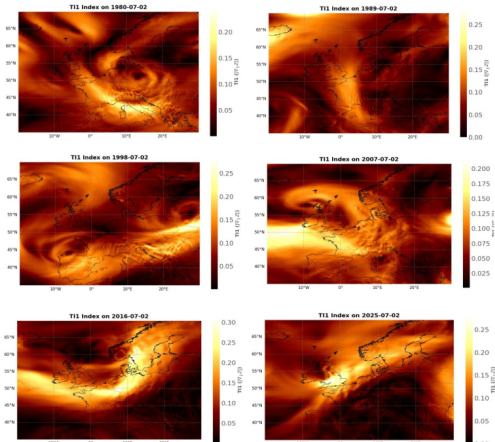


Table:  $TI1 = |\nabla z| = \sqrt{\left(\frac{\partial z}{\partial x}\right)^2 - \left(\frac{\partial z}{\partial y}\right)^2}$ , dimensionless proxy of thermal wind strength at 500 hPa height.

# Final conclusions

- 1 **The Euclid. distances figure** showed how similar or dissimilar daily atmospheric circulation patterns are to each other. Being it a left-skewed one, many days are similar to one another → common patterns.
- 2 How “tight” the computed **analog**s are in the feature space is found by the magnitude of distances. Namely the kernel density estimate computed with seaborn utilities.
- 3 If most distances are **low** → high pattern similarity, possibly dominated by a few regimes.
- 4 If distances vary **widely** → strong variability, with many rare patterns.
- 5  $q=0.98$ , the analogs will lie in the left tail of this distribution, namely the most similar maps. The linear fit and CI computed indicated a **consistent trend**. Further investigation on larger and more broad datasets is needed (namely the other indexes reported before).
- 6 **TI1 remarks**, its higher values match stronger horizontal gradients → stronger baroclinicity  
 $\propto \frac{1}{\rho^2} \vec{\nabla} \rho \times \vec{\nabla} p$  mainly a raw indicator of CAT events occurrence.

Quantile ( $q$ )	Slope	95% Confidence Interval	Ref. day
0.98	17,903.600	(9,140,823, 26,666,377)	16619
0.99	8,792.900	(4,424,833, 13,160,967)	16619
0.995	4,756.900	(2,318,860, 7,194,940)	16619

**Table:** Slope coefficients and 95% confidence intervals for different quantile thresholds ( $q$ ) corresponding to reference day 16619.

# Bibliography

-  Alberti, T., Faranda, D., Rapella, L., Coppola, E., Lepreti, F., Dubrulle, B., and Carbone, V. (2024). Impacts of changing atmospheric circulation patterns on aviation turbulence over europe. *Geophysical Research Letters*, 51(23):e2024GL111618. e2024GL111618 2024GL111618.
-  Ellrod, G. P. and Knapp, D. I. (1992). An objective clear air turbulence forecasting technique: Verification and operational use. *Weather and Forecasting*, 7(1):150 – 165.
-  Faranda, D., Messori, G., Coppola, E., Alberti, T., Vrac, M., Pons, F., Yiou, P., Saint Lu, M., Hisi, A. N. S., Brockmann, P., Dafis, S., Mengaldo, G., and Vautard, R. (2024). Climameter: contextualizing extreme weather in a changing climate. *Weather and Climate Dynamics*, 5(3):959–983.
-  Sharman, R., Tebaldi, C., Wiener, G., and Wolff, J. (2006). An integrated approach to mid and upper level turbulence forecasting. *Weather and Forecasting*, 21(3):268 287.